Research Article | Vol. 24, No. 19 | 19 Sep 2016 | OPTICS EXPRESS 22210

Optics EXPRESS

Transverse single-shot cross-correlation scheme for laser pulse temporal measurement via planar second harmonic generation

B. WANG,[1] C. COJOCARU,[1,*] W. KROLIKOWSKI,[2,3] Y. SHENG,[2] AND J. TRULL[1]

[1]*Departament de Física, Universitat Politècnica de Catalunya, Terrassa 08222, Barcelona, Spain*
[2]*Laser Physics Centre, Research School of Physics and Engineering, Australian National University, Canberra, ACT 0200, Australia*
[3]*Science Program, Texas A&M University at Qatar, Doha, Qatar*
**crina.maria.cojocaru@upc.edu*

Abstract: We present a novel single-shot cross-correlation technique based on the analysis of the transversally emitted second harmonic generation in crystals with random distribution and size of anti-parallel nonlinear domains. We implement it to the measurement of ultrashort laser pulses with unknown temporal duration and shape. We optimize the error of the pulse measurement by controlling the incident angle and beam width. As novelty and unlike the other well-known cross correlation schemes, this technique can be implemented for the temporal characterization of pulses over a very wide dynamic range (30 fs–1ps) and wavelengths (800–2200 nm), using the same crystal and without critical angular or temperature alignment.

OCIS codes: (190.0190) Nonlinear optics; (190.2620) Harmonic generation and mixing, (190.4420) Nonlinear optics, transverse effects in; 230.4320 Nonlinear optical devices.

References and links

1. J.-C. Diels and W. Rudolph, *Ultrashort Laser Pulse Phenomena*, 2nd Ed. (Academic Press, 2006).
2. K. Oba, P. C. Sun, Y. T. Mazurenko, and Y. Fainman, "Femtosecond single-shot correlation system: a time-domain approach," Appl. Opt. **38**(17), 3810–3817 (1999).
3. I. Walmsley and C. Dorrer, "Characterization of ultrashort electromagnetic pulses," Adv. Opt. Photonics **1**(2), 308–437 (2009).
4. J. C. Diels, J. J. Fontaine, I. C. McMichael, and F. Simoni, "Control and measurement of ultrashort pulse shapes (in amplitude and phase) with femtosecond accuracy," Appl. Opt. **24**(9), 1270–1282 (1985).
5. R. Trebino, K. W. DeLong, D. N. Fittinghoff, J. N. Sweetser, M. A. Krumbügel, and D. J. Kane, "Measuring ultrashort laser pulses in the time-frequency domain using frequency-resolved optical gating," Rev. Sci. Instrum. **68**(9), 3277 (1997).
6. B. Alonso, I. J. Sola, Ó. Varela, J. Toro, C. Mendez, J. San Román, A. Zaïr, and L. Roso, "Spatiotemporal amplitude-and-phase reconstruction by Fourier-transform of interference spectra of high-complex-beams," J. Opt. Soc. Am. B **27**(5), 933–940 (2010).
7. B. Yellampalle, R. D. Averitt, and A. J. Taylor, "Unambiguous chirp characterization using modified-spectrum auto-interferometric correlation and pulse spectrum," Opt. Express **14**(19), 8890–8899 (2006).
8. G. Szabó, Z. Bor, and A. Müller, "Phase-sensitive single-pulse autocorrelator for ultrashort laser pulses," Opt. Lett. **13**(9), 746–748 (1988).
9. J. Paye, M. Ramaswamy, J. G. Fujimoto, and E. P. Ippen, "Measurement of the amplitude and phase of ultrashort light pulses from spectrally resolved autocorrelation," Opt. Lett. **18**(22), 1946–1948 (1993).
10. C. Yan and J. C. Diels, "Amplitude and phase recording of ultrashort pulses," J. Opt. Soc. Am. B **8**(6), 1259–1263 (1991).
11. F. Salin, P. Georges, G. Roger, and A. Brun, "Single-shot measurement of a 52-fs pulse," Appl. Opt. **26**(21), 4528–4531 (1987).
12. R. Trebino, "FROG. The measurement of ultrashort laser pulses," (Springer, 2000).
13. M. Beck, M. G. Raymer, I. A. Walmsley, and V. Wong, "Chronocyclic tomography for measuring the amplitude and phase structure of optical pulses," Opt. Lett. **18**(23), 2041–2043 (1993).
14. L. Gallmann, D. H. Sutter, N. Matuschek, G. Steinmeyer, U. Keller, C. Iaconis, and I. A. Walmsley, "Characterization of sub-6-fs optical pulses with spectral phase interferometry for direct electric-field reconstruction," Opt. Lett. **24**(18), 1314–1316 (1999).
15. G. Berden, S. P. Jamison, A. M. MacLeod, W. A. Gillespie, B. Redlich, and A. F. van der Meer, "Electro-optic technique with improved time resolution for real-time, nondestructive, single-shot measurements of femtosecond electron bunch profiles," Phys. Rev. Lett. **93**(11), 114802 (2004).

#272275 http://dx.doi.org/10.1364/OE.24.022210
Journal © 2016 Received 25 Jul 2016; accepted 4 Sep 2016; published 15 Sep 2016

Optics EXPRESS

16. D. H. Auston, "Measurement of picosecond pulse shape and background level," Appl. Phys. Lett. **18**(6), 249 (1971).
17. G. Priebe, K. Janulewicz, V. Redkorechev, J. Tummler, and P. Nickles, "Pulse shape measurement by a non-collinear third-order correlation technique," Opt. Commun. **259**(2), 848–851 (2006).
18. Y. Wang, J. Ma, J. Wang, P. Yuan, G. Xie, X. Ge, F. Liu, X. Yuan, H. Zhu, and L. Qian, "Single-shot measurement of $>10^{10}$ pulse contrast for ultra-high peak-power lasers," Sci. Rep. **4**, 3818 (2014).
19. J. Trull, I. Sola, B. Wang, A. Parra, W. Krolikowski, Y. Sheng, R. Vilaseca, and C. Cojocaru, "Ultrashort pulse chirp measurement via transverse second-harmonic generation in strontium barium niobate crystal," Appl. Phys. Lett. **106**(22), 221108 (2015).
20. V. Roppo, D. Dumay, J. Trull, C. Cojocaru, S. M. Saltiel, K. Staliunas, R. Vilaseca, D. N. Neshev, W. Krolikowski, and Y. S. Kivshar, "Planar second-harmonic generation with noncollinear pumps in disordered media," Opt. Express **16**(18), 14192–14199 (2008).
21. J. Trull, S. Saltiel, V. Roppo, C. Cojocaru, D. Dumay, W. Krolikowski, D. Neshev, R. Vilaseca, K. Staliunas, and Y. S. Kivshar, "Characterization of femtosecond pulses via transverse second-harmonic generation in random nonlinear media," Appl. Phys. B **95**(3), 609–615 (2009).
22. W. Wang, K. Kalinowski, V. Roppo, Y. Sheng, K. Koynov, Y. Kong, C. Cojocaru, J. Trull, R. Vilaseca, and W. Krolikowski, "Second- and third-harmonic parametric scattering in disordered quadratic media," J. Phys. At. Mol. Opt. Phys. **43**(21), 215404 (2010).

1. Introduction

Lasers delivering ultrashort pulses play nowadays an increasingly important role in many research and technological fields. Material processing, high-resolution imaging and detection, investigation of complex molecular system's dynamics, biomedical science and medicine are only few examples where the interaction of femtosecond light pulses with different media is the main tool. These applications are meaningful only if one is able to perfectly characterize the laser pulses used in the experiment. Most of the parameters such as the peak power, spectral bandwidth, chirp content or M^2 factor strongly depend on the temporal duration and shape of the pulse [1]. The femtosecond time scale is beyond the reach of standard electronic display instruments. Many different techniques, most widely based second harmonic generation (SHG) correlations, have been extensively adopted for a partial or complete temporal characterization of ultrashort laser pulses [2–11]. Among them, techniques based on frequency resolved optical-gating (FROG and XFROG), or on spectral interferometry (SPIDER) allow for a detailed reconstruction of the pulse characteristics, both in amplitude and phase [12–14]. Beside these complex and expensive techniques, classical auto-correlation is still a valuable tool in many situations where only partial information such as pulse duration is required. When the temporal pulse shape has to be also retrieved, cross-correlation techniques between the unknown pulse and a selected reference are usually implemented [15–18]. Since these methods relay on the detection of the second harmonic (SH) generation, the requirement of phase matching critical alignment, temperature tuning and the need of using very thin crystals make them far from user-friendly.

Few years ago, a novel auto-correlation scheme based on the detection of the transverse second harmonic signal generated by the overlapping of two non-collinear laser beams in a nonlinear crystal with a random-sized domain distribution, has been proposed as a simple and effective single-shot technique for the partial temporal characterization of Gaussian pulses with duration from 30 fs up to few hundreds of fs [19–21]. The particular two-dimensional (2D) distribution of the needle-like, oppositely oriented nonlinear domains in specific ferroelectric crystals creates a continuous set of reciprocal lattice vectors with different modulus and orientations within the plane perpendicular to the optical axis, providing phase matching for nonlinear frequency conversion over a very broad wavelength and angular range [22]. The SH is generated in a whole plane perpendicular to the input pulse propagation direction, including the transverse one, making possible the detection of the transverse second harmonic generated (TSHG) signal. These transverse autocorrelation (TAC) technique removes the demand of thin nonlinear crystals or critical angular and/or temperature tuning needed in traditional AC setups. Moreover, recording the auto-correlation trace from the top of the crystal (transverse direction) allows following the evolution of the AC trace all along the propagation distance within the crystal.

In this work we implement, for the first time to our knowledge, the transverse single-shot cross-correlation technique (TSCC) to the measurement of the duration and shape of

Optics EXPRESS

ultrashort non-Gaussian laser pulses. This method combines the capability of typical cross-correlation methods, where the spatially resolved nonlinear signal generated by the overlap between a reference and an unknown pulse provides information of the temporal cross-correlation signal, with the advantages of the transverse detection of the cross-correlation trace provided by our TAC technique. Finally, we study and optimize the limitations imposed by the pulse duration.

2. Experimental configuration, results and discussions

Our experimental set-up is schematically shown in Fig. 1. The pulse to be measured (P) (from now on called "unknown" pulse) is combined with a reference pulse (R) in a characteristic single-shot cross-correlation scheme (Fig. 1(a)). Both pulses overlap with an external angle of 2α within a Strontium Barium Niobate (SBN) crystal. The crystal shows as-grown random-sized nonlinear domains with an inverted sign of the 2nd order nonlinearity, oriented along the optical axis (z-axis in Fig. 1). The non-collinear interaction between the two pulses generates a SH signal which, due to the characteristics of the SBN crystal, is emitted in a whole plane (xy) perpendicular to the one containing both propagating beams and the optical axis z. The TSHG is schematically shown in the Fig. 1(b). A CCD camera placed above the crystal records the spatially resolved TSH signal generated by the two pulses along the whole propagation distance within the crystal. A typical TSH trace recorded by the CCD camera is shown in the inset of the Fig. 1(b). This signal represents the spatial intensity cross-correlation trace, $I_{CC}(z)$, directly related to the temporal intensity cross-correlation $I_{CC}(t)$. To retrieve the temporal cross-correlation trace from the corresponding spatially dependent one, a calibration factor, depending on the geometry of the setup, must be applied. This calibration can be properly obtained by measuring the auto-correlation of the reference pulse, as detailed in [22]. The cross-correlation signal intensity $I_{CC}(t)$ between the reference pulse with the intensity $I_R(t)$ and the unknown pulse $I_P(t)$ can be mathematically represented by their convolution. So the unknown pulse $I_P(t)$ can be retrieved if we assume the reference temporal profile is known using the relation:

$$I_P(t) = \mathcal{F}^{-1}\left(\frac{\mathcal{F}(I_{CC}(t))}{\mathcal{F}(I_R(t))}\right) \tag{1}$$

where $\mathcal{F}$ and $\mathcal{F}^{-1}$ denote the Fourier transform and inverse Fourier transform operators.

In our experiment we have used pulses at 800 nm provided by a Ti:Sapphire laser working at 76 MHz, with a duration of 180 fs (at FWHM) and energies of 20 nJ/pulse. The pulse was divided into two identical replicas using a beam splitter. One of the replicas served as reference pulse (R) while the second one was used to generate the "unknown" pulse. In this work, since we want to explore and prove the capabilities and resolution of our technique for the temporal profile measurement, we have used a controllable "unknown" pulse. For this purpose we have built a double-Gaussian pulse generator, based on a Michelson-type configuration, generating a controllable pulse profile from the overlapping of two temporally delayed Gaussian pulses (A and B in Fig. 1(a)). The delay between the two pulses (T_{sep}) was carefully controlled moving the mirror M_1 with a high precision motorized linear stage over a distance D_{sep}, with 0.1 μm step resolution. $T_{sep} = 2D_{sep}/c$, where c is the speed of light. The reference and the double-peak unknown pulse were then overlapped inside a 5 mm long SBN crystal with an external intersection angle $\alpha = 25°$. The TSHG signal at 400 nm was recorded using a Spiricon SP620U CCD camera with 230 px/mm resolution, placed above the crystal. Two half-wavelength plates were used to control the polarization of the beams incident onto the SBN for maximizing the efficiency of the SH process (ee-e interaction).

Optics EXPRESS

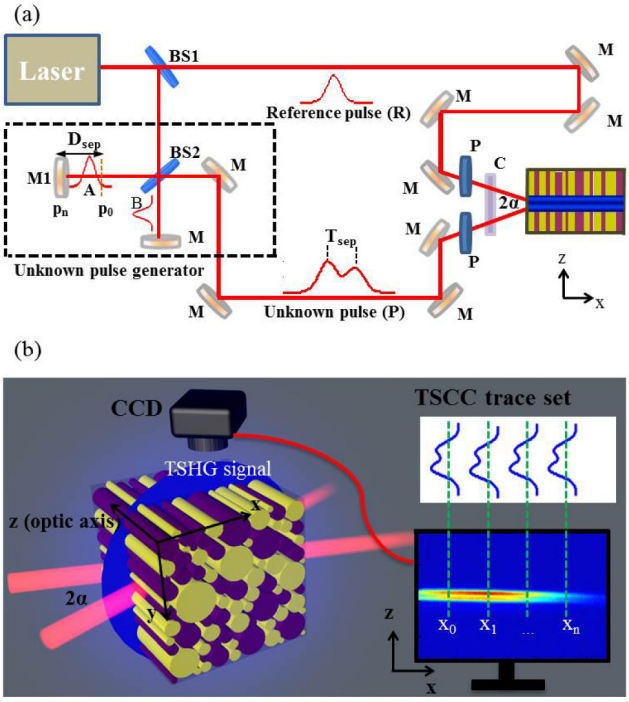

Fig. 1. (a) Schematic representation of the TSCC setup; (b) The unknown pulse is overlapped with the reference pulse and focused onto the SBN crystal with the intersect angle 2α; the vertical emitted TSHG signal from the top of the SBN crystal is detected by a CCD; the TSCC trace sequence at different x position (x_0, x_1…x_n) constitute the TSCC trace set.

As a first step we have to calibrate the "unknown" pulse. Zero delay calibration was obtained by scanning mirror M_1 until the CCD image of TAC trace formed by the reference signal R and signal A overlapped completely with the CCD image of TAC trace formed by signal R and signal B. This measurement served to characterize the reference beam and provided the calibration factor between the spatial and temporal domains by using the relation (2), as detailed in [21]:

$$T_{AC} = \frac{2\Delta z_{AC} \sin\alpha}{c} \tag{2}$$

where Δz_{AC} is the FWHM width of the TAC trace sequence recorded by the CCD, while TAC is the FWHM duration of the TAC temporal signal. The obtained space-time decoding factor was 19.4 fs/pixel (1 pixel equal to 19.4 fs). This value will set the resolution of our measurements in this particular configuration.

Experimental measurements of the TAC trace corresponding to the reference pulse are shown in Fig. 2(a) where the TAC signal at position x = 2 mm (Fig. 2(b)) shows a reference pulse FWHM duration in intensity of T = 178 fs. The recorded images correspond to that shown in the inset of Fig. 1(b) and have been zoomed in the transverse direction in Figs. 2 and 3. Note that the apparent tilting of the traces is due to the fact that we used different scale in the x and z directions in the plots in order to show better the transverse dependence of the I_{CC} traces. The experimental cross-correlation trace between the R pulse and the P pulse for T_{sep} = 300 fs is shown in Fig. 2(c). The cross-correlation profile at the position x = 2 mm is plotted in Fig. 2(d), where the two-peaked asymmetric cross-correlation trace of the unknown pulse can be clearly seen.

Optics EXPRESS

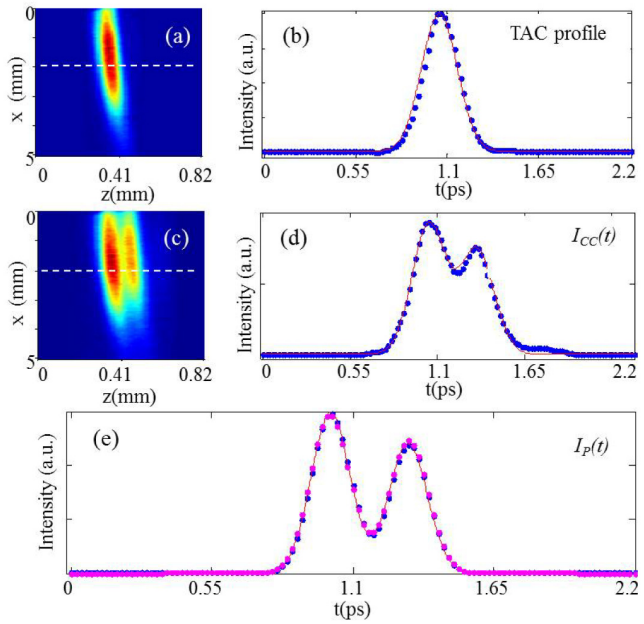

Fig. 2. (a): The CCD recorded TAC trace set along the 5 mm SBN crystal; (b): The TAC trace sequence at $x = 2$ mm; (c): The CCD recorded TSCC trace set along the 5 mm SBN crystal; (d): $I_{CC}(t)$, the TSCC trace sequence at $x = 2$ mm; (e): $I_P(t)$, the retrieved unknown pulse sequence (blue dots), the Gaussian analytical fit (continuous red line), the original "unknown" pulse (pink dots) plotted used the experimental values of T_{sep} and the pulse duration for each single pulse measured in Fig. 2(b).

Using the same calibration factor obtained in the TAC measurement, one can directly retrieve the temporal cross-correlation profile, $I_{CC}(t)$, from the spatially resolved measurement $I_{CC}(z)$. Note that this technique permits to observe the evolution of the cross-correlation trace (transverse profile in z direction) along the crystal propagation distance (x direction). Since the incident pulses are affected by material dispersion during propagation inside the crystal, a dynamical evolution of the pulses can be detected and used to determine the pulse chirp as shown in [20]. This fact becomes relevant for pulses shorter than 100fs, but it is not a limiting factor in our experiment where dispersion lengths are of the order of $L_D = 25$ mm or larger.

The unknown temporal profile can be retrieved from the deconvolution between the $I_{CC}(t)$ experimental data and the reference pulse, using Eq. (1). We have observed that direct use of discrete experimental profile data leads to the appearance of oscillations in the retrieved signal profile. We have used the following procedure to obtain a smooth temporal profile: *i)* obtain a fit of the experimental temporal cross-correlation and get a smooth function of $I_{CC}(t)$; *ii)* obtain a fit of the reference pulse and *iii)* use these fitting functions to retrieve the temporal pulse profile using Eq. (1).

In principle, any fitting algorithm could be used to obtain a smoothed version of the experimental data. Here we use fitting functions for the cross-correlation data corresponding to a superposition of two Gaussian functions as follow:

$$I_{CC}(t) = I_A \exp\left(-\frac{(t-t_0)^2}{\left(T_{cc}/\left(2\sqrt{\ln 2}\right)\right)^2}\right) + I_B \exp\left(-\frac{(t-t_0-T_{sepcc})^2}{\left(T_{cc}/\left(2\sqrt{\ln 2}\right)\right)^2}\right) \quad (3)$$

where T_{sepcc} is the pulses separation and T_{cc} the individual pulse duration at FWHM in intensity.

Figure 2(d) shows the fitted curve in red where T_{cc} = 250 fs and the temporal separation T_{sepcc} = 299 fs. The reference pulse was fitted using a Gaussian function:

Optics EXPRESS

$$I_{R(t)} = \exp\left(-\frac{(t-t_0)^2}{\left(T_R/\left(2\sqrt{\ln 2}\right)\right)^2}\right) \tag{4}$$

with T_R = 178 fs.

Using these two functions and applying the deconvolution procedure we have obtained the retrieved unknown temporal pulse shown in Fig. 2(e) (blue dots). From the corresponding fit (red line), using the same functional form as the Eq. (3), we can directly determine the unknown pulse peak separation T_{sepP} = 299 fs and the temporal duration of each individual Gaussian pulse, T_P = 175 fs. These results are in very close agreement with the real values used in our experiment for the generation of the unknown pulse, T_{sep} and T.

An estimated error ε between the retrieved values and the values set for the generation of the unknown pulse is calculated by using the following expression:

$$\varepsilon = \sqrt{\frac{\left(T_{sepP} - T_{sep}\right)^2}{T_{sep}^2} + \frac{\left(T_P - T\right)^2}{T^2}} \tag{5}$$

giving, in this particular case, a value of 1.9%.

We have generated several different double-peak pulses setting T_{sep} to 200, 267, 367, 1333 fs. Figures 3(a1)-3(a4) show the CCD recorded TSCC traces set along the SBN crystal for each pulse. The corresponding cross-correlation signals selected at x = 2 mm position, are shown in Figs. 3(b1)-3(b4) together with the fitted curves (red line). The retrieved unknown temporal pulses are shown in Fig. 3(c1-c4). The errors obtained for each case using Eq. (5) are 4.4%, 1.4%, 0.6% and 9.9% respectively, showing that the longer the pulse the larger the error, keeping all values under a 10%.

Once we have described the capabilities of the method to measure the transverse cross-correlation traces, in order to check our experimental results and to identify limitations of the technique we numerically solved the nonlinear interaction (in the phase-matching regime) and propagation of the reference and unknown pulses through the SBN crystal to obtain the cross-correlation trace. For short pulses, the material dispersion acting during propagation along the crystal leads to a pulse lengthening, which affects the trace profile during propagation. This effect can be used to determine the chirp parameter of the pulse incident in the crystal as has been demonstrated in [19]. However for the purpose of this work, the pulses used where so long that no significant dispersion effects were expected. In the case of long pulses the factor that cannot be overlooked in order to obtain a valid measurement is the effect of the beam size on the recorded trace.

To check the relevance of this effect in our particular configuration, we should consider the beam size relative to the pulse duration. In a previous work [21] we discussed two extreme situations: when the condition $T_R/R_0 << \tan(\alpha/c)$ holds (R_0 is the spatial FWHM width in intensity, for our laser beam R_0 = 1mm) the I_{CC} provides the direct mapping of the temporal pulse shape, with no limitation imposed by the finite beam size. In the case $T_R/R_0 >> \tan(\alpha/c)$, the CCD recorded TSCC trace sequence I_{CC} does not give a proper TAC because the beam size limits the overlapping region.

Optics EXPRESS

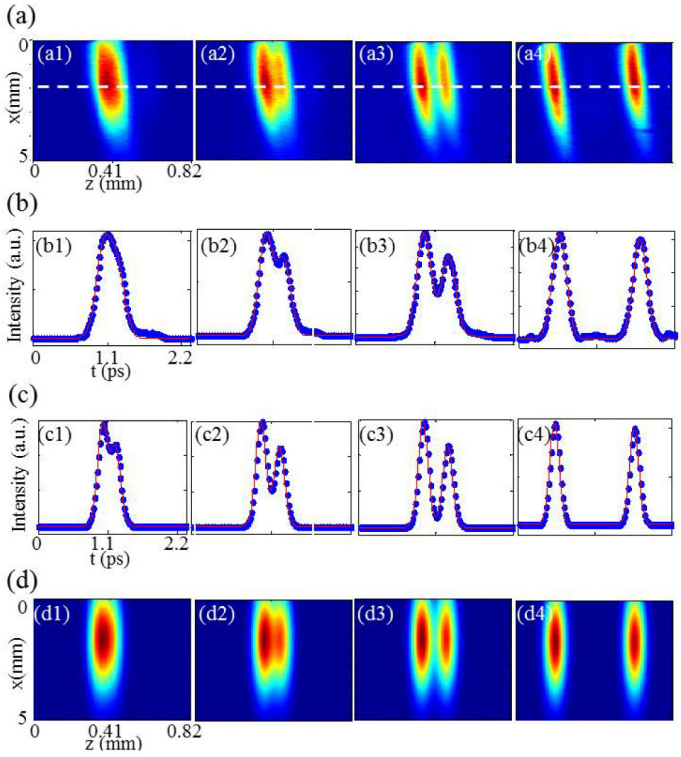

Fig. 3. (a) The CCD recorded TSCC traces set along the 5-mm SBN crystal when the Tsep are 200, 267, 367, 1333 fs respectively; (b): The TSCC profiles at the marked position in (a); (c): the retrieved shaped pulse sequence; (d): the simulated TSCC trace set along the 5-mm SBN crystal.

Due to the duration of our pulses we need to consider these effects in our actual setup. We extended the TAC trace simulation method in [21] to obtain the TSCC trace recorded in our experiment. The reference and unknown pulse can be written respectively as:

$$I_R = \exp\left(-\frac{z_1^2}{\left(R_0/\left(2\sqrt{\ln 2}\right)^2\right)}\right)\exp\left(-\frac{(t-x_1/2)^2}{T_R/\left(2\sqrt{\ln 2}\right)^2}\right) \tag{6}$$

$$I_P = \exp\left(-\frac{z_2^2}{\left(R_0/\left(2\sqrt{\ln 2}\right)\right)^2}\right)\left[I_C\exp\left(-\frac{(t-x_2/2)^2}{T_P/\left(2\sqrt{\ln 2}\right)^2}\right)+I_D\exp\left(-\frac{(t-T_{sepP}-x_2/2)^2}{T_P/\left(2\sqrt{\ln 2}\right)^2}\right)\right]s \tag{7}$$

where (x_1, z_1) and (x_2, z_2) are coordinate systems oriented along the propagation direction of each one of the beams; T_R and T_P are the FWHM duration in intensity measured for the reference and unknown pulses; T_{sepP} is the experimentally retrieved unknown pulse peak separation and u is the velocity of the pulse in the SBN crystal.

By considering that the ee-e interaction is phase-matched in our crystal by the random domains and after performing a change of variables to a common reference system (x,z), the recorded TSCC trace set can be simulated by:

$$I_{CC} = d_{33}\int I_R I_P dt \tag{8}$$

the I_{CC} represented by Eq. (8) can be written as the product of two functions, one related to the spatial characteristics, $I_{spatial}$

Optics EXPRESS

$$I_{spatial}(\alpha, R_0) = \exp\left(-2\frac{z^2\cos(\alpha)^2 + x^2\sin(\alpha)^2}{\left(R_0/\left(2\sqrt{\ln 2}\right)\right)^2}\right) \quad (9)$$

and the time integral of the temporal component of I_{CC}, $I_{temporal}$, the I_{CC} represented by Eq. (8) can then be rewritten as:

$$I_{CC} = I_{spatial}(\alpha, R_0)\, I_{temporal}(\alpha) \quad (10)$$

When $T_P/R_0 << \tan\alpha/u$, the spatial part can be safely approximated by 1 and the I_{CC} is decided solely by $I_{temporal}$ which is the direct mapping of the temporal pulse shape. When $T_P/R_0 >> \tan\alpha/u$, the TSCC trace sequence I_{CC} is strongly affected by $I_{spatial}$. As can be seen in this expression, the influences of this term will depend strongly on the incident angle of the overlapping beams.

In order to further analyze the effect of the incident angle and beam diameter on the TSCC trace, we simulated the particular case where T_R = 180 fs; T_P = 180 fs; T_{sepP} = 300 fs; I_C/I_D = 0.8. The simulated $I_{temporal}$, $I_{spatial}$ and I_{CC} traces for different incident angles and beam diameters are shown in Fig. 4. The first column, (a_1), (b_1) and (c_1) shows the temporal cross-correlation of the pulse with no spatial contribution for two different incidence angles 12° (a_1) and 30° (b_1-c_1) evidencing the role played by the incidence angle. Temporal broadening is not observed during propagation due to the long pulses used in the simulation (notice that for such pulse durations the group velocity dispersion length is L_D = 190 mm for the cross-correlation signal). The second column (a_2), (b_2) and (c_2) shows the effect of the spatial part ($I_{spatial}$) for three different situations: (a_2): α = 12°, R_o = 0,8 mm; (b_2): α = 30°, R_o = 0,3 mm and (c_2): α = 30°, R_o = 0,8 mm. The finite size of the beam leads to a strong reduction of the overlapping region, so the TSCC trace remains unchanged only at a particular region where $I_{spatial}$ is approximately 1. The effect of the spatial part depends strongly on the beam diameter and incidence angle. The third column (a_3), (b_3) and (c_3) shows the complete TSCC trace set, I_{CC} given by Eq. (10).

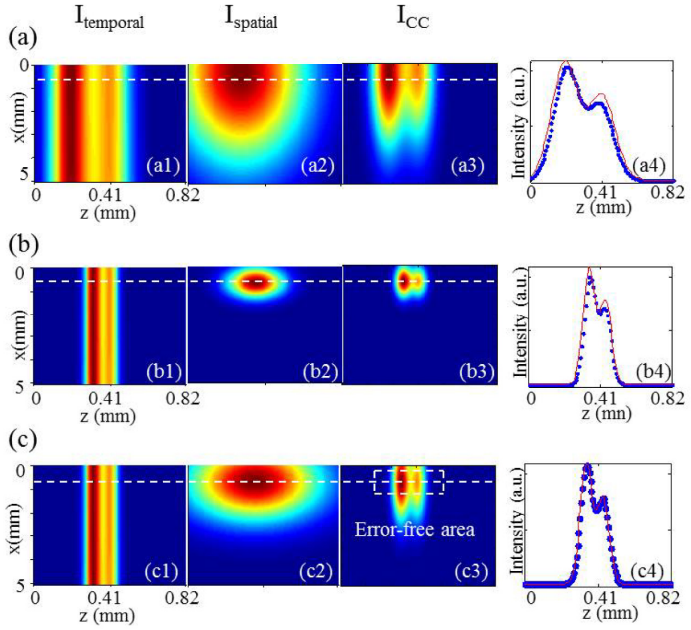

Fig. 4. Simulation of the temporal part of the I_{CC} trace: (a_1) $I_{temporal}$ (α = 12°, R_0 = 0.8mm); (b_1) $I_{temporal}$ (α = 30°, R_0 = 0.3mm); and (c_1) $I_{temporal}$ (α = 30°, R_0 = 0.8mm). Simulation of the spatial part: (a_2) $I_{spatial}$ (α = 12°, R_0 = 0.8mm); (b_2) $I_{spatial}$ (α = 30°, R_0 = 0.3mm); and (c_2) $I_{spatial}$ (α = 30°, R_0 = 0.8mm); Total cross-correlation trace, I_{CC}, for each case [(a_3), (b_3) and (c_3)]. Profiles of the CC trace at the position of the dashed line for $I_{temporal}$ (red line) and I_{CC} (blue dots) [(a_4), (b_4) and (c_4)].

Optics EXPRESS

Last column in Fig. 4 shows the trace at the position indicated by the dashed white line of $I_{temporal}$ (red line) and I_{CC} (blue dots) for each one of the situations. As we can see in plot (a_4), a too small angle is limiting the capability to record properly the TSCC trace sequence so the blue dots do not match the temporal CC signal given by the red line. For the case of plot (b_4), a too small beam radius leads to a narrow $I_{spatial}$ component, which also leads to a failure in the TSCC reconstruction. As the pulses to be measured become longer, one should increase the incident angle or/and expand the beam diameter to get an error-free TSCC trace set. The plot in (c_4) shows that if the conditions of beam radius and incidence angle are adequate one can properly record the proper CC trace.

The experimental values of beam radius and incidence angle were selected according to these considerations. The simulated TSCC traces obtained using the retrieved values of pulse duration, T_P, and peak separation of the unknown pulses, T_{sepP}, after the deconvolution process (with the values of incidence angle and beam radius used in the experiment) are shown in Fig. 3(d1-d4) respectively, showing very good agreement with the experimental recorded TSCC traces of Fig. 3(a). The increased error with unknown pulse duration mentioned in a previous paragraph could be due to the fact that increasing the pulse duration we are approaching the limit imposed by the spatial part of I_{CC}.

3. Conclusions

In conclusion, we demonstrate that using a nonlinear SBN crystal and the corresponding TSHG, we performed transverse cross-correlation single-shot measurements and we can characterize the duration and temporal shape of ultrashort laser pulses with complex temporal profiles. Using this procedure, one could measure TSCC traces for pulses ranging between 30 fs up to 1 picosecond. We have measured several two-peaked Gaussian beams over a broad temporal window and studied the role played by factors such as the incident angle or beam radius as error sources for the final resolution of this pulse measurement technique. We have shown that, if we want to perform measurements in the long pulse duration range an increase of the incident angle or/and an expansion of the beam diameter would be required. In this technique the vertical emission of TSHG removes the requirement of a thin nonlinear crystal and enables one to measure the undistorted pulse at the entrance of the crystal. As important characteristic, the property of automatic phase matching without angular alignment or temperature control, makes the technique applicable to a very broad wavelength range and enormously simplifies the operation process.

Acknowledgments

We acknowledge financial support by Spanish Ministerio de Educación y Ciencia (project FIS2015-65998-C2-1-P (MINECO/FEDER)), US ACQRDECOM (projects W911NF-11-1-0387 and W911NF-12-1-0201) and Generalitat de Catalunya (2014 SGR-957). B. Wang is supported by the Erasmus Mundus Doctorate Program "Europhotonics" 2013-2016. Y. Sheng and W. Krolikowski acknowledge support of Australian Research Council and Qatar National Research Fund (NPRP 09-020-1-006).